RESEARCH ARTICLE

VOLCANICA

Submitted: 2026-02-10 | Accepted: 2026-06-25 | Published: 2026-07-02

# Plumbing system dynamics during the 2024 paroxysmal sequence at the Voragine crater of Mt. Etna volcano as revealed by the olivine crystal cargo

Massimiliano Cardone[α], Giorgio Costa[α], Marisa Giuffrida*[α], and Marco Viccaro[α,β]

[α] Università degli Studi di Catania, Dipartimento di Scienze Biologiche Geologiche e Ambientali, Catania, Italy.

[β] Istituto Nazionale di Geofisica e Vulcanologia—Sezione di Catania, Osservatorio Etneo, Catania, Italy.

## Abstract

The sequence of six paroxysmal eruptions that occurred between July and August 2024 at Mt. Etna's Voragine crater has been investigated in order to constrain the plumbing system dynamics. Whole-rock and glass major-element analyses have been integrated with a detailed petrological study of erupted products, focusing on olivine major-element compositions to track magma storage and transfer dynamics leading to the eruptions. Olivine chemistry and thermodynamic modeling indicate an intermediate reservoir at ~2.7 km b.s.l. as the main magma storage region. Fe–Mg diffusion chronometry on zoned olivines constrains magma transfer timescales, suggesting mafic recharge from depths of 6–8 km b.s.l. over 3–4 months, followed by progressive replacement of magmas occupying the shallower levels 1–3 weeks before the onset of Strombolian activity in mid-June. Compared to the last lava fountain activity at Voragine in 2015–2016 and the long-lasting sequence at South East Crater in 2020–2022, the 2024 magmas underwent slower transfer from depth and longer residence at intermediate storage levels, suggesting important modifications in the working modes of the current plumbing system.

Keywords: Etna; Voragine; Plumbing system; Paroxysmal eruption; Olivine zoning; Diffusion chronometry.

## 1 Introduction

Volcanic activity at Mt. Etna has been the focus of extensive and continuous multidisciplinary monitoring during the last 30 years, encompassing geophysical, geochemical, and petrological observations [Patanè et al. 2003; Bonaccorso et al. 2004; Caltabiano et al. 2004; Métrich et al. 2004; Cannata et al. 2018; Borzi et al. 2020; Paonita et al. 2021; Bonaccorso et al. 2025]. This long-term effort has provided an exceptional dataset for tracking the temporal evolution of eruptive activity and for constraining processes governing magma storage, transfer, and eruption dynamics. Volcanological models carried out over the last several decades converge to depict the Mt. Etna plumbing system as a complex, multi-level, vertically extended network of variably connected sill-like storage regions and dykes extending down to depths of approximately 30 km [Lo Bue et al. 2024; Palano et al. 2024; Del Piccolo et al. 2025]. In this context, the petrology of erupted products has greatly contributed to recognizing depth of storage and tracking the ascent path of magma within the plumbing system [Armienti et al. 1989; Corsaro et al. 2007; Corsaro and Miraglia 2014; Giuffrida and Viccaro 2017; Ubide and Kamber 2018; Giuffrida et al. 2021; 2023; Corsaro et al. 2024]. In particular, the knowledge of pre-eruptive magma dynamics has rapidly increased due to the systematic application of diffusion chronometry to chemically zoned crystals [Kahl et al. 2011; 2015; Viccaro et al. 2016; Giuffrida and Viccaro 2017; Giuffrida et al. 2021; 2023]. Applications to volcanic minerals from the recent eruptive record of Etna indicate the occurrence of frequent episodes of mafic replenishments that may involve different storage regions at different crustal depths, mobilizing more evolved resident magmas before eruptions. Modes and timescales over which these processes occur differ from eruption to eruption. However, significant phases of deep recharge with activation of the deepest reservoirs and very rapid ascent of primitive melts were found to characterize the onset of high intensity explosive eruptions at Etna [Giuffrida and Viccaro 2017; Cannata et al. 2018; Giuffrida et al. 2023].

Lava fountain episodes characterized by intense explosive activity have become very frequent at Etna since the late 1980s [Behncke and Neri 2003; Andronico and Corsaro 2011]. Among the summit craters, the South East Crater (SEC) has been the most productive, generating over two hundred events clustered in sequences lasting weeks to years [La Delfa et al. 2001; Behncke et al. 2006; Andronico and Corsaro 2011; Behncke et al. 2014; Giuffrida and Viccaro 2017; Andronico et al. 2021; Giuffrida et al. 2023]. Less frequent, but particularly powerful, lava fountain activity occurred at the crater Voragine (VOR) on July 22, 1998 [Aloisi et al. 2002], September 4, 1999 [Harris and Neri 2002] and more recently in short sequences of multiple events during December 3–5, 2015 [four events; Corsaro et al. 2017], May 18–21, 2016 [three events; Edwards et al. 2018], and finally between July 4 and August 15, 2024 with a sequence of six events. Despite the relative rarity of high-intensity eruptions, episodes of renewed activity at VOR have commonly marked major transitions in Etna's activity, leading to substantial changes in eruptive behavior and morphological modifications of the volcano summit [Corsaro et al. 2017; Pompilio et al. 2017; Cannata et al. 2018; Giuffrida et al. 2021].

The reawakening of VOR in 2024 occurred after a long period of volcanic dormancy lasting over six months. The

* marisa.giuffrida@unict.it

Editor: A. Jeffery | Production: B. Hosseini; G. Seropian

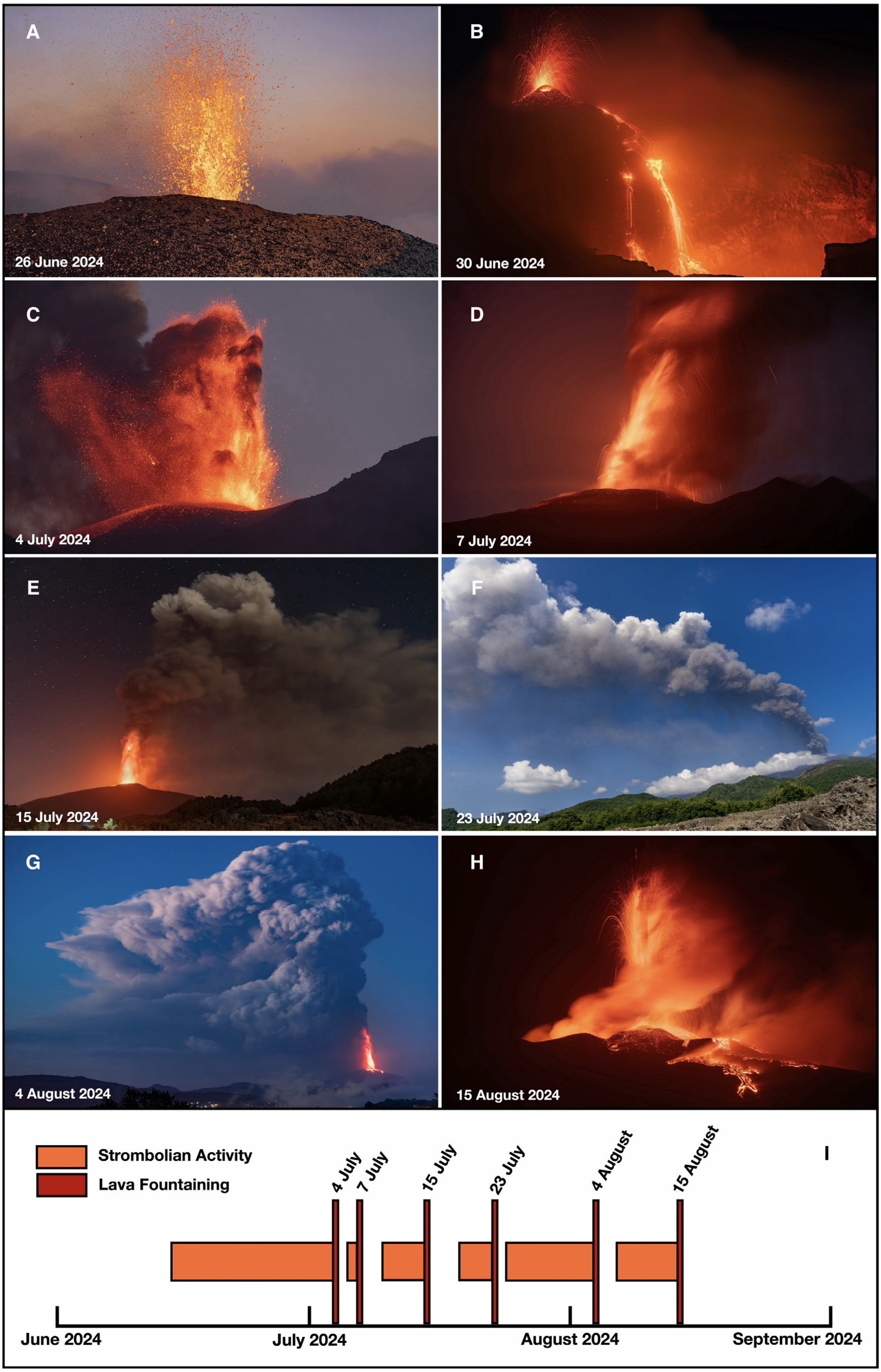


Figure 1: (Caption next page.)

Figure 1: (Previous page.) Sequence of photographs illustrating the main stages of eruptive activity at the Voragine crater (VOR) during the summer of 2024. [A] Mild Strombolian activity in the afternoon of June 26, observed from the western rim of the VOR. [B] Intensification of the Strombolian activity and emplacement of an intra-crateric lava flow spilling from the VOR into the adjacent Bocca Nuova crater (BN), observed in the evening of June 30. [C] The first paroxysmal eruption in the afternoon of July 4. [D] The second paroxysmal eruption at dawn on July 7. [E] The third paroxysmal eruption in the evening of July 15. [F] Eruptive column produced during the fourth paroxysmal eruption on the morning of July 23. [G] Eruptive column produced during the fifth paroxysmal eruption at dawn on August 4. [H] The sixth paroxysmal eruption during the night between August 14 and 15, with the lava flow directed toward the western flank of the volcano. [I] Timeline of the VOR eruptive activity during the summer of 2024.

Table 1: List of the six paroxysmal eruptions that occurred at the Voragine crater (VOR) during 2024 showing details about the timing and duration of the lava fountains, along with height of the eruptive columns generated during each episode. The time of starting and ending of the lava fountaining phase and the height of the eruptive columns are derived from the volcanic activity reports published by the INGV—Etnean Observatory available at www.ct.ingv.it.

| Episode number | Date (dd/mm/yyyy) | Sample | Start of lava fountain (UTC) | End of lava fountain (UTC) | Duration (minutes) | Eruptive column height (m) |
|---|---|---|---|---|---|---|
| 1 | 04/07/2024 | VOR_040724 | 16:15[1] | 01:50[1] | 545 | ~4500 |
| 2 | 07/07/2024 | VOR_070724 | 02:00[1] | 08:00[1] | 360 | ~9000 |
| 3 | 15/07/2024 | VOR_150724 | 18:45[2] | 23:40[2] | 305 | ~8000 |
| 4 | 23/07/2024 | VOR_230724 | 05:40[3] | 08:15[3] | 155 | ~8000 |
| 5 | 04/08/2024 | VOR_040824 | 03:20[4] | 08:10[4] | 290 | ~10000 |
| 6 | 14/08/2024 | VOR_140824 | 22:30[5] | 01:20[5] | 170 | ~9500 |

[1]INGV-OE [2024a] [2]INGV-OE [2024b] [3]INGV-OE [2024c] [4]INGV-OE [2024d] [5]INGV-OE [2024e]

crater produced modest Strombolian explosions starting from mid-June 2024. Strombolian explosions gradually intensified over time, eventually turning into a new spectacular sequence of lava fountains. The six paroxysmal events that occurred between July and August 2024 at VOR are the focus of the present study. Specifically, this work aims to shed light on the chemical and physical factors that led to the onset of this new sequence of violent eruptions at VOR. We provide a petrological investigation of volcanic tephra not only erupted during the paroxysmal events, but also related to the phase of Strombolian activity of June 15 to July 4 that preceded the onset of paroxysmal eruptions on July 4, 2024. Specifically, the study combines the whole rock data of the six paroxysms with micro-analytical data acquired on volcanic crystals and glasses from both the Strombolian activity and the paroxysmal episodes. The investigation primarily focuses on the microanalysis of olivine crystals to assess their major element variation from core to rim. This allowed the application of Fe–Mg diffusion models to retrieve timescales of the pre-eruptive magma storage and transfer. This approach pursues a crystal chemistry-based investigation strategy already consolidated for the study of the Etna plumbing system [cf. Giuffrida et al. 2023, and references therein], which enables a comprehensive assessment of the spatial and temporal evolution of the volcano storage and transfer zones. The approach therefore makes possible consistent comparison with past activities, facilitating the evaluation of the short to long term changes in the working modes of Mt. Etna.

## 2 The volcanic activity of Voragine during 2024

The crater VOR was in a state of rest for several years prior to the summer of 2024. The latest volcanic manifestations occurred between September 2019 and February 2021. However, this eruption was only characterized by persistent Strombolian activity of variable intensity, with two main phases identified between September 2019 and April 2020, and between December 2020 and February 2021, occasionally accompanied by intra-crateric lava effusion and intermittent fumarolic degassing [Giuffrida et al. 2021].

Following this period, no further magmatic activity was recorded at VOR until June 2024, when mild spattering activity suddenly resumed without specific precursory signals. The reawakening started on June 14 and progressively intensified, transitioning from spattering to Strombolian explosions over the following weeks (Figure 1A). This process led to the growth of a new intra-crateric cone and was accompanied by the emission of small lava flows that spilled into the adjacent Bocca Nuova crater (BN; Figure 1B).

On the afternoon of July 4, Strombolian explosions increased in both frequency and intensity, culminating at ~15:15 UTC in the first paroxysmal episode of the sequence (Figure 1C; Table 1). This event lasted approximately 9 hours and was characterized by sustained lava fountains reaching 400–500 m in height and the emission of an eruptive column that rose to ~4.5 km a.s.l. [INGV-OE 2024a]. During this episode, an intra-crateric lava flow was emplaced, filling both crater depressions within BN. Lava fountaining ceased at approximately 02:00 UTC on July 5. On July 6, sporadic

Table 2: Thermodynamic parameters determined by Giuffrida et al. [2023] for the magmatic environments involved in the post-2015 eruptions at Mt. Etna volcano. $M_i$ indicates the magmatic environment; $H_2O$ and $CO_2$ intervals refer to the volatile content dissolved in the melt of a specific $M_i$.

| $M_i$ | Fo (mol%) | $T$ (°C) | $P$ (MPa) | $fO_2$ (bars) | $H_2O$ (wt.%) | $CO_2$ (wt.%) |
|---|---|---|---|---|---|---|
| $M_{00}$ | 84–83 | 1144 | 275 | 1.70E–08 | 2.51–2.60 | 0.18–0.16 |
| $M_0$ | 82–80 | 1131 | 242 | 1.20E–09 | 2.60–2.63 | 0.16–0.14 |
| $M_{1a}$ | 79–77 | 1110 | 207 | 1.86E–10 | 2.64–2.68 | 0.12–0.11 |
| $M_{1b}$ | 76–74 | 1088 | 115 | 3.09E–11 | 2.40–2.50 | 0.10–0.07 |
| $M_2$ | 73–68 | 1065 | 50 | 1.26E–11 | 2.58–2.52 | 0.05–0.04 |

Strombolian activity resumed, gradually intensifying during the early hours of July 7 and culminating at approximately 02:30 UTC in the second paroxysmal episode (Figure 1D). This event produced lava fountains up to 600–700 m in height and an eruptive column that reached ~9 km a.s.l. [INGV-OE 2024a]. During the final stages of the episode, a lava flow descended several hundred meters from the western rim of BN. This paroxysmal eruption lasted ~5 hours, ending at approximately 07:30 UTC. The eruptive activity at VOR resumed again on July 9 and intensified during the early hours of July 11, producing high-energy Strombolian explosions and a modest lava flow extending a few hundred meters westward. In this case, the activity did not evolve into lava fountaining and instead gradually declined in intensity, although it never ceased completely. On the afternoon of July 15, Strombolian explosions at VOR again increased in both frequency and intensity, culminating at ~20:15 UTC in the third paroxysmal episode of the sequence (Figure 1E). This event showed similar characteristics to the previous ones, with high lava fountains reaching ~800 m, an eruptive column rising to ~8 km a.s.l. [INGV-OE 2024b], and a lava flow directed toward the western flank. The paroxysmal phase lasted nearly three hours, ending at approximately 23:15 UTC. The fourth paroxysmal episode was preceded by renewed explosive activity at VOR starting on July 18, which gradually intensified in the subsequent days and transitioned into a paroxysmal phase at approximately 05:45 UTC on July 23 (Figure 1F). The most energetic phases of this episode produced lava fountains up to ~1 km in height and an eruptive column reaching ~8 km a.s.l. [INGV-OE 2024c]. This episode had shorter duration compared to the previous ones, ceasing around 07:45 UTC. Just over 24 hours later, the prelude of the fifth paroxysmal episode began. Unlike the preceding events, this episode was characterized by a fast escalation from the Strombolian activity to sustained lava fountaining within some tens of minutes. The climax occurred between 03:00 and 07:10 UTC on August 4 (Figure 1G), with lava fountains exceeding 1.5 km in height and an eruptive column that rose to ~10 km a.s.l. [INGV-OE 2024d]. Two lava flows were emplaced during this event: the first resulted from an overflow at the western rim of BN, while the second was generated by the accumulation of the still-fluid pyroclastic material on the western flank of VOR. The final eruptive episode of the sequence was preceded by a new phase of escalating explosive activity that began on August 6, culminating in a paroxysmal phase at approximately 22:30 UTC on August 14 (Figure 1H). During the most intense phase, lava fountains reached ~1.5 km in height and the eruptive column rose to ~9.5 km a.s.l. [INGV-OE 2024e]. Additionally, a new eruptive fissure opened along the morphological saddle between VOR and North East Crater (NEC), producing a lava flow that partially filled the NEC crater depression. A second more voluminous lava flow was emplaced on the western flank of the volcano. The paroxysmal phase lasted approximately three hours and ended at 01:30 UTC on August 15, marking the end of this cycle of eruptions.

# 3 Methods

## 3.1 Sampling and analytical procedures

Nine sets of tephra samples were collected on the southern flank of Mt. Etna during the eruptive activity. Three sets are related to the Strombolian activity preceding the first paroxysm, namely VOR_160624, VOR_250624, and VOR_040724_STR, whereas the other six sets of samples belong to the six paroxysmal eruptions that occurred at VOR (Table 1). Major element compositions of the whole rock were analyzed for each of the paroxysm samples at SGS Laboratories in Toronto (Canada) using X-ray fluorescence spectroscopy (WD-XRF) on powdered pellets, with corrections applied for matrix effects. The loss on ignition (LOI) was measured gravimetrically at 1000°C for 24 hours and the quality of the whole rock data was evaluated through analyses on the standards OREAS751 and SARM32, ensuring analytical precision and the accuracy of major element concentrations of 2–3%. All the whole rock analyses are available in the Supplementary Material 1. Thin sections were examined using both optical and scanning electron microscopy at the Earth Science section of the Department of Biological, Geological and Environmental Sciences at the University of Catania. Backscattered electron images and micro-chemical analyses were acquired on 106 olivine crystals along core-to-rim profiles with spacing between analytical spots of ~3–6 µm. Analyses were performed with a Tescan Vega-LMU scanning electron microscope equipped with an EDAX Neptune XM4-60 microanalyzer, employing an energy-dispersive system (EDS) with an ultra-thin Be window. Major element measurements in the mineral phases and volcanic glasses were carried out using accelerating voltage of 20 kV and beam current set to 2 nA. To maintain accuracy throughout the analyses, repeated measurements were performed on the certified reference glass and olivine of the SPI 02753-AB Serial KF standards, resulting in a precision of 3–5% for major elements. All the analyses per-

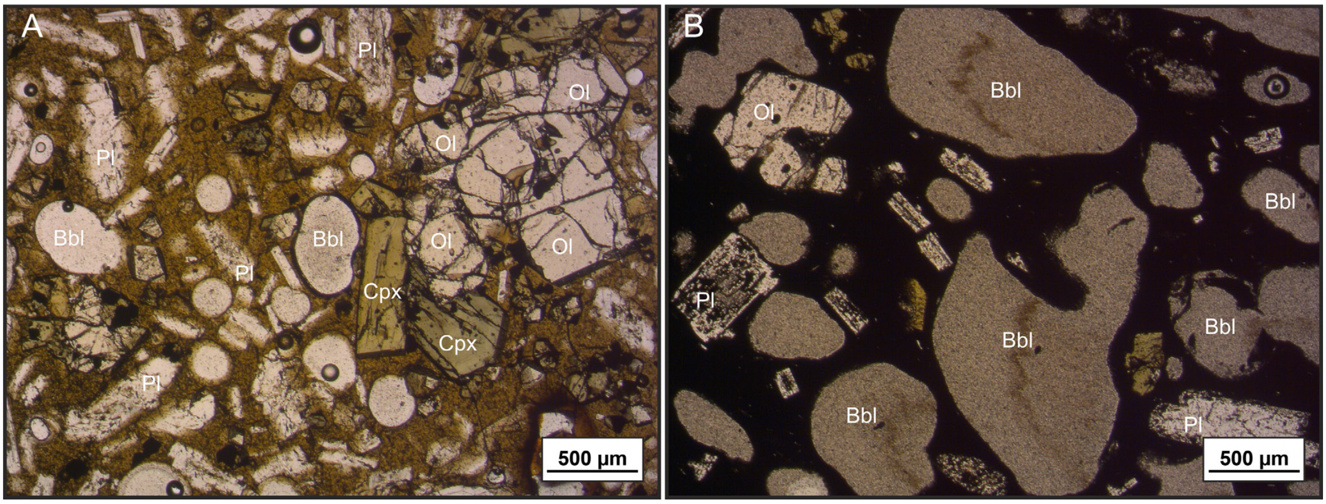


Figure 2: Thin section under plane-polarized light (PPL) of: [A] scoria from June 25 Strombolian activity (VOR_250624) and [B] lapilli from July 7 paroxysm (VOR_070724B). Annotations indicate: Pl—plagioclase; Ol—olivine; Cpx—clinopyroxene; Bbl—vesicles.

formed on mineral phases and volcanic glasses are available in Supplementary Materials 1–2.

### 3.2 Fe–Mg diffusion modeling strategy

The interdiffusion of Fe–Mg was modeled in 23 selected crystals through a finite-difference numerical model operating in one dimension [Costa et al. 2008, Supplementary Material 3]. The analytical strategy was guided by strict geometric and crystallographic criteria. Since evident obliquity in sectioning (>45° with respect to the *c*-axis) and off-center cuts can profoundly distort the shape of compositional profiles and the retrieved diffusion timescales [Shea et al. 2015a; b], very small grains (<100 μm) were systematically excluded, as they typically correspond to peripheral sections. Similarly, profiles intersecting crystal corners, where overlapping diffusion domains may falsely elongate calculated timescales, were discarded [Shea et al. 2015b].

Each analyzed crystal was characterized crystallographically through conoscopic inspection under polarized light using a Zeiss four-axis universal stage. This procedure allowed the determination of the angular relationship between the *a*, *b*, and *c* axes and the diffusion transects. These geometric parameters are required to account for the anisotropic nature of Fe–Mg diffusion in olivine and are used to correct diffusion coefficients following Dohmen and Chakraborty [2007]. The modeling was employed on crystals oriented close to the *c*-axis direction, where diffusion is fastest and most efficient [Costa and Chakraborty 2004]. Fe–Mg diffusion coefficients were determined by using the thermodynamic parameters (temperature $T$, pressure $P$ and oxygen fugacity $fO_2$; Table 2) characterizing compositionally-distinct magmatic environments of olivine crystallization beneath Etna, as determined by Giuffrida et al. [2023]. Each zoned profile was always modeled using the average $T$, $P$ and $fO_2$ of the final environment where the olivine shows evidence of chemical relaxation after intrusion. As initial conditions, we used a homogeneous profile for modeling simple normally or reversely zoned chemical gradients. A step-like initial distribution, assuming a maximum concentration range at the boundary layer, was instead adopted in the presence of chemical gradients (normal or reverse) that became smoother or flat at the rim, which suggest the rim grew after the crystal was incorporated and re-equilibrated into an environment having thermodynamic characteristics different than the initial crystallization environment. In all cases, diffusion was assumed to occur under isothermal conditions and fixed concentration conditions were imposed at the crystal boundaries.

The uncertainty in diffusion timescales was quantified by propagating the errors associated with the diffusion parameters, following the procedure proposed by Kahl et al. [2015]. Uncertainties of ±20°C in temperature and $\pm 1 \times 10^{-10}$ bars in oxygen fugacity were considered for the calculation on the basis of the ranges in temperature and oxygen fugacity calculated thermodynamically for Etna's magmatic environments by Giuffrida et al. [2023]. The derived diffusion times should be interpreted as maximum times, under the assumption that compositional zoning evolved exclusively through diffusive processes, rather than crystal growth or resorption [Costa et al. 2008].

## 4 Results

### 4.1 Petrography of the 2024 Voragine volcanic products

Samples from the June–August volcanic activity at VOR show variable modal abundances of crystals, with plagioclase being the dominant phase (~50–65%), followed by augitic clinopyroxene (20–35%), olivine (5–10%) and Fe–Ti oxides (~5%). We observed noticeable textural differences at the microscale in whole rock and crystals between samples belonging to the preparatory Strombolian activity (June 16, 25 and July 4) and samples related to the paroxysms (July 4, 7, 15, 23 and August 4, 14), with those from the Strombolian activity of July 4 showing intermediate features.

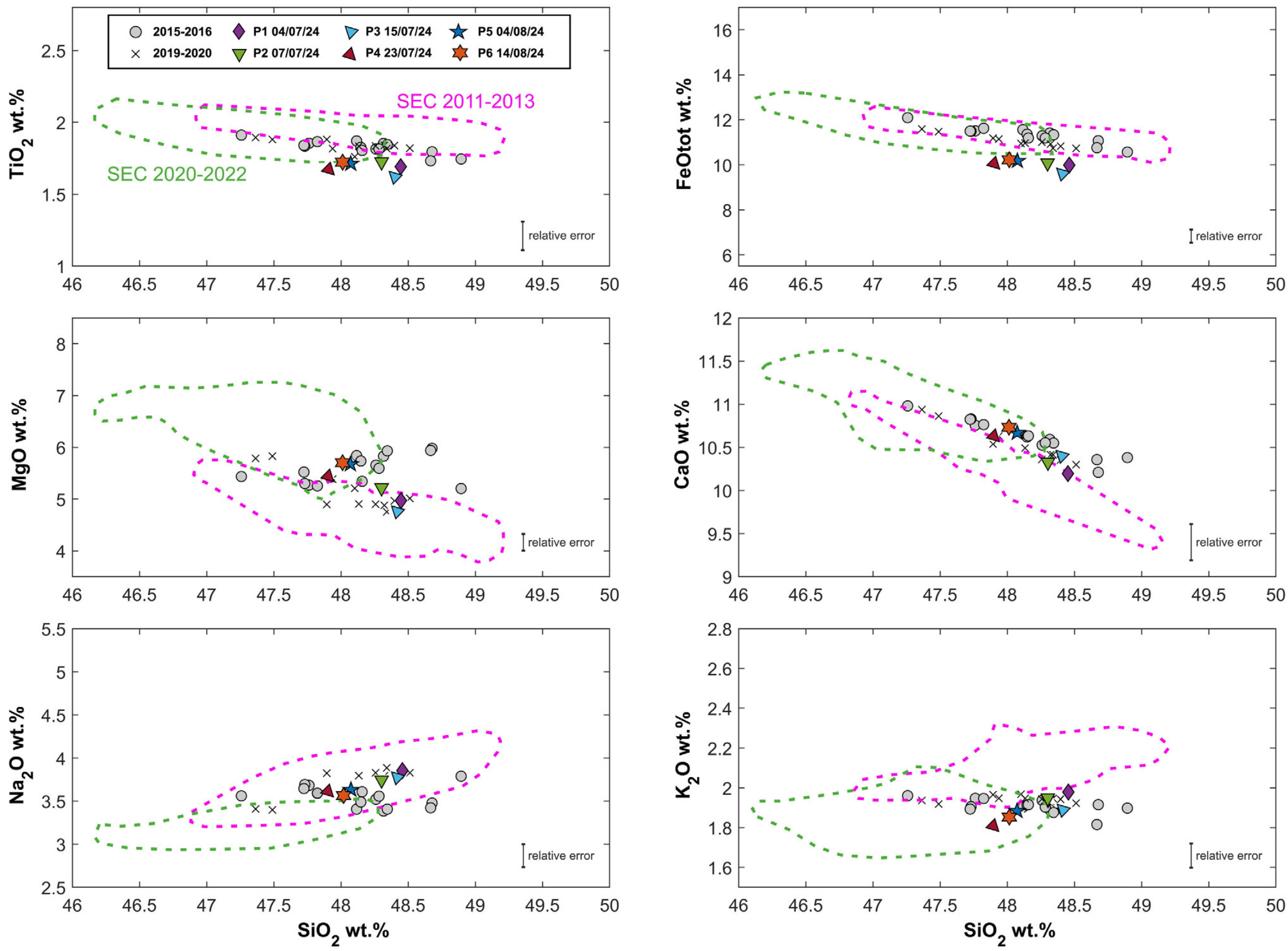


Figure 3: Whole-rock major oxide compositions of products from the 2024 paroxysmal events (P1 to P6) at Voragine (VOR), compared with those erupted at the VOR during 2015–2016 (gray circles; Cannata et al. [2018]) and 2019–2020 (black crosses; Giuffrida et al. [2021]). Whole-rock compositions of tephra erupted during the paroxysmal sequences at the South East Crater (SEC) in 2011–2013 [Giuffrida and Viccaro 2017] and 2020–2022 [Giuffrida et al. 2023] are also shown as pink and green dashed fields, respectively. Error bars represent the analytical uncertainty associated with the major oxide concentrations measured in the products of the 2024 paroxysmal activity.

Samples related to the Strombolian activity show a seriate porphyritic texture with crystals of various sizes measured along the major axis: phenocryst (>0.3 mm), microphenocryst (0.1–0.3 mm) and a glassy brownish matrix characterized by the presence of microlites (<0.1 mm) of plagioclase and augitic clinopyroxene (Figure 2A). The microlite content in the matrix is significantly high in products of July 4. Plagioclases in all samples of the Strombolian activity have euhedral habits with major axis length varying between 150 µm and ~1 mm. Pervasive disequilibrium textures (sieve textures) occur at plagioclase cores and less frequently at rims. Olivine phenocrysts are subhedral to euhedral with size varying between 200 µm and ~1 mm, while augitic clinopyroxenes show an average size of 250 µm with the presence of few millimetric specimens in euhedral to subhedral habits. The presence of olivine glomerocrysts (Figure 2A) was observed, along with frequent Fe–Ti oxides and augitic clinopyroxene glomerocrysts.

Tephra samples from the paroxysmal events show significantly lower phenocryst contents (10–15%), while retaining the same mineral assemblage and a similar seriate grain-size distribution to that observed in tephra from the Strombolian phase. Although the relative proportions of the phenocryst phases remain broadly comparable, tephra from paroxysms exhibit higher plagioclase abundance, reaching up to 65 vol%, with plagioclase occurring predominantly as microlites. Disequilibrium textures are rare and, when present, only affect the plagioclase core (Figure 2B). Subhedral to euhedral olivines and augitic clinopyroxene are ~250 µm in size, only rarely forming large individual crystals (>500 µm) or glomerocrysts.

## 4.2 Geochemistry of the 2024 Voragine volcanic products

Whole rock chemical analyses for major elements were performed on samples from the six paroxysmal events (Supplementary Material 1). Results in Figure 3 show that most major oxides (e.g. MgO, CaO, $Na_2O$, $K_2O$) follow differentiation

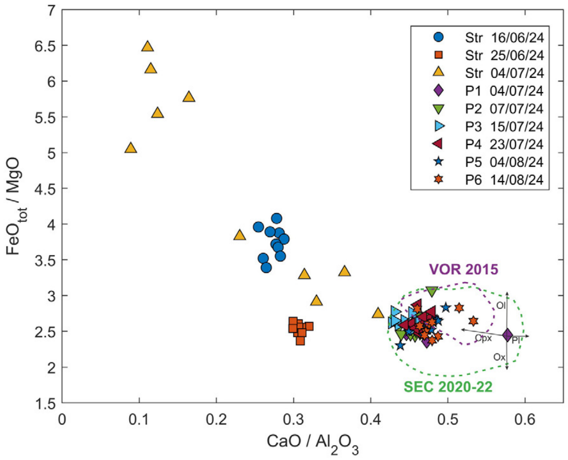


Figure 4: $FeO_{tot}/MgO$ vs. $CaO/Al_2O_3$ ratios for residual glasses from the three samples belonging to Strombolian events preceding paroxysms (Str) and the six paroxysmal eruptions (P) occurring at Voragine crater (VOR) during 2024. Fields delimited by colored dashed lines refer to the glass compositions of December 2015 VOR eruptive products [Pompilio et al. 2017] and to the 2020–2022 paroxysmal sequence at the South East Crater (SEC) [Giuffrida et al. 2023]. Vectors indicate how composition would vary if 5% of clinopyroxene, 10% of plagioclase, 5% of olivine or 3% of Ti-magnetite is fractionated from the least evolved glass composition measured.

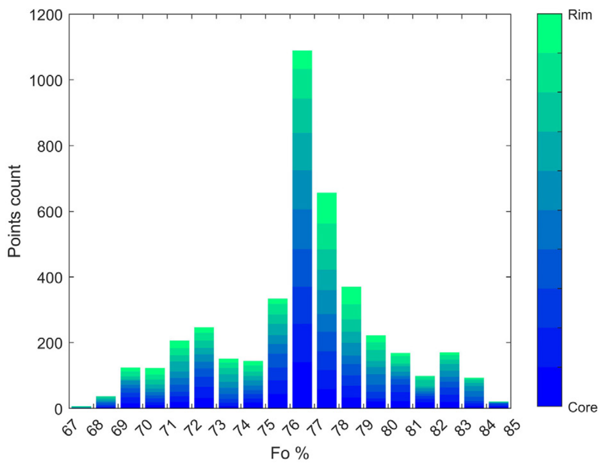


Figure 5: Frequency histogram of the micro-analytical data (total = 4268 points) obtained on olivine crystals in products of the 2024 Voragine (VOR) activity showing the distribution of forsterite contents. The color bar indicates the normalized position of each analysis along the compositional profiles, where each increment corresponds to 10% of the crystal length from core to rim.

trends consistent with those of products erupted during the previous VOR activity of 2015–2016 and 2019–2020 [data from Cannata et al. 2018; Giuffrida et al. 2021]. Iron and titanium oxides display slightly lower concentrations, within the relative error, when compared to products previously erupted at VOR, a feature attributed to analytical bias given that these products were analyzed through WD-XRF in a different laboratory. Furthermore, we report higher values for LOI compared to the usual values observed at Mt. Etna since 2011 (average of 1.25 wt.%), spanning from 1.2 to 1.9 wt.%. Notably, the least evolved products (i.e. lower $SiO_2$ and higher MgO contents) correspond to the last three paroxysms, whereas the most evolved compositions are associated with the first three events. Figure 4 shows the composition of VOR 2024 volcanic glasses for tephra erupted during the Strombolian phase and those related to paroxysmal eruptions along with glass compositions from Voragine 2015 [Pompilio et al. 2017] and the 2020–2022 paroxysmal sequence at the SEC [Giuffrida et al. 2023] for comparison. The compositions are plotted in the diagram $FeO_{tot}/MgO$ vs. $CaO/Al_2O_3$ which can be a proxy of the glass evolution through the June to August VOR eruptive activity. Excluding the Strombolian activity of July 4, the most evolved glasses correspond to the Strombolian activity of June 16, followed by a progressive shift towards more mafic compositions during the July 4 paroxysm (Figure 4). Indeed, we note that data from the Strombolian activity of July 4 are more scattered, a feature probably measured due to the presence of high numbers of microlites in the matrix which could affect the composition of the surrounding glass. Finally, the six paroxysms of the VOR 2024 sequence partially overlap the more evolved compositions deriving from the activity of both VOR 2015 and SEC 2020–2022.

### 4.3 Olivine composition and zoning patterns

Microanalysis was conducted on 106 olivine crystals along core-to-rim profiles: 25 of the analyzed olivines come from tephra of the Strombolian phase, while 81 olivines were derived from tephra of the paroxysmal eruptions. The chemical variability within olivine is illustrated in Figure 5, where spot analyses for the forsterite content (Fo = Mg/[Mg+Fe+Mn] mol%) are counted and grouped into stacked columns according to their position along the profiles. Most olivine crystals (49% of the total dataset) exhibit Fo core compositions (blue shades in Figure 5) in the range $Fo_{76–78}$, showing an almost unimodal distribution among the samples. Cores at $Fo_{71-73}$ and $Fo_{82–83}$ occur with minor frequency of 10% and 7%, respectively. Core compositions lower than $Fo_{71}$ and higher than $Fo_{83}$ are rare and appear generally distributed around the main peak of frequency. Rim compositions (green shades in Figure 5) cluster within Fo intervals that closely resemble those observed at the crystal cores. In particular, 65% of the olivines display rim compositions between $Fo_{76–79}$, while 15% fall within the $Fo_{70–73}$ range.

Olivine crystals are classified in three olivine populations (OP; Figure 6) that are defined on the basis of the chemically homogeneous inner cores with flat Fo profiles (i.e. chemical plateau). This feature was observed in a total of 84 crystals distributed as follows: 14% cores at $Fo_{80–84}$ constituting OP1, 70% at $Fo_{75–79}$ defining OP2, and 16% at $Fo_{68–73}$ representing OP3.

The shape of compositional profiles from core to rim defines four different zoning patterns: (a) non-zoned crystals that show a slight normal or reverse trend (~1 Fo%) at the outer rim

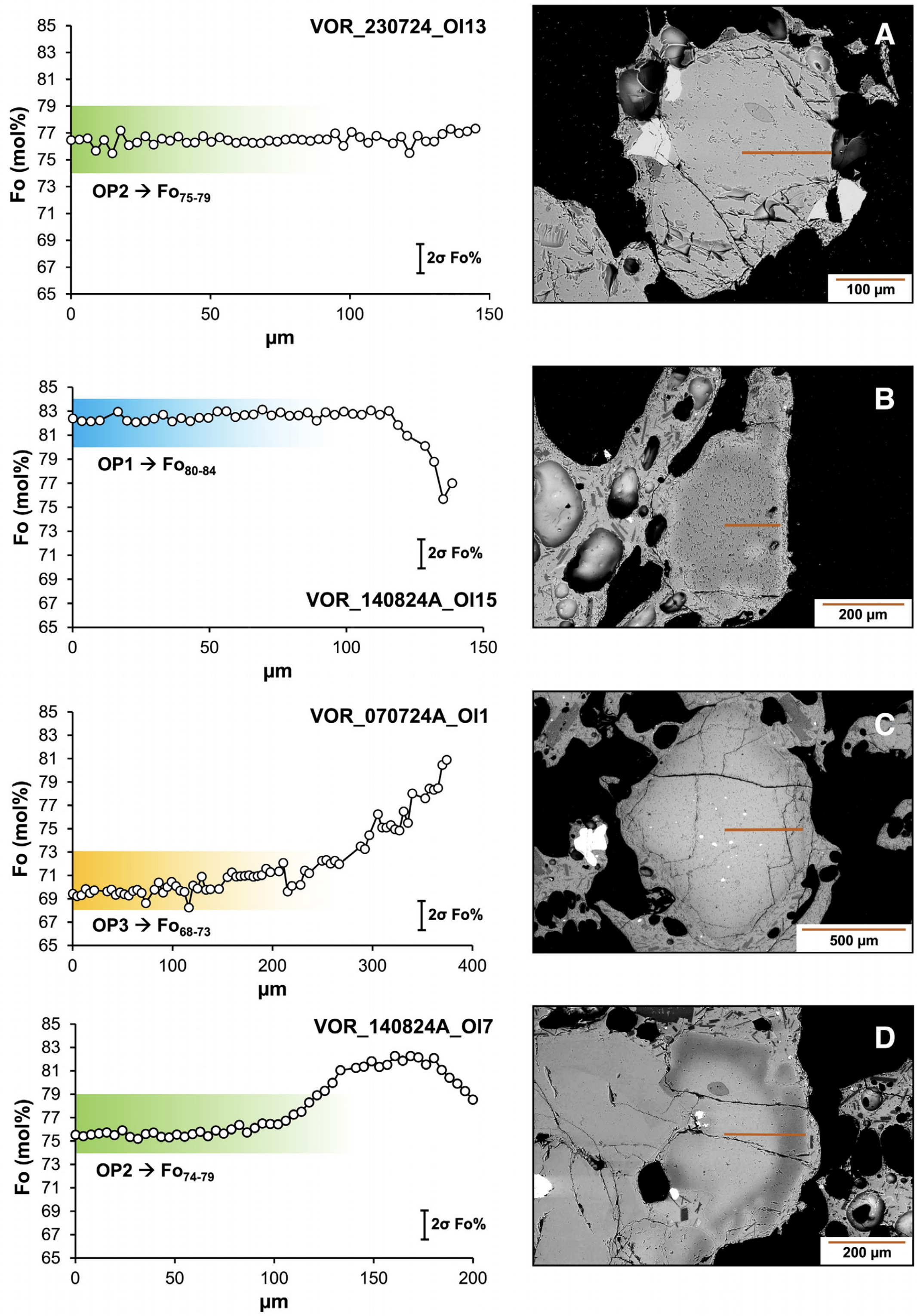


Figure 6: Olivine compositional profiles showing examples of plateaus that define olivine populations, together with the four zoning types recognized within the 2024 eruptive sequence at the Voragine crater (VOR). [A] Crystal belonging to OP2 showing zoning type 1 (non-zoned profile); [B] Crystal belonging to OP1 showing zoning type 2 (normal zoning); [C] Crystal belonging to OP3 showing zoning type 3 (reverse zoning); [D] Crystal belonging to OP2 showing zoning type 4 (complex zoning). Backscattered electron (BSE) images and the corresponding profile traces are shown for each crystal. All chemical profiles were measured from the crystal core (0 µm) to the outer rim. The shaded colored bands indicate the Fo intervals associated with the core plateaus of distinct olivine populations.

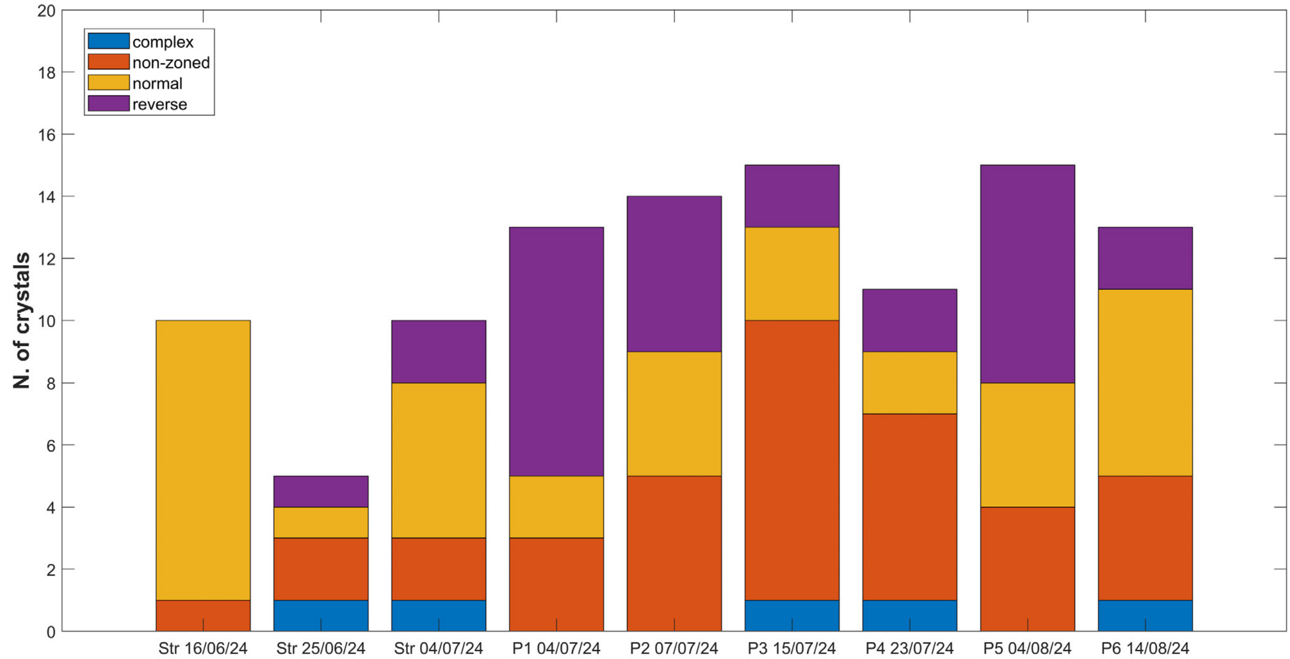


Figure 7: Stacked histogram showing the distribution of olivine crystals with different zoning types in products erupted throughout the June to August 2024 volcanic activity at Voragine (VOR). The $x$-axis reports the reference dates, with Str indicating Strombolian activity and P indicating paroxysmal eruptions.

(Figure 6A); (b) normal zoning with Fo concentration gradually decreasing from the core towards the rim (Figure 6B); (c) reverse Fo zoning (Figure 6C); (d) complex profiles that show reverse zoning shifting to normal towards the crystal edge (Figure 6D). Non-zoned and normally zoned profiles are the most frequent within samples, with each pattern characterizing 34% of crystals, followed by reverse zoning (27%), whereas complex zoning is rare (5%). The distribution of these zoning patterns throughout the eruptive period is displayed in Figure 7. In particular, the abundance of non-zoned crystals within the investigated samples progressively increases from June 16 to July 15, reaching here its maximum and then decreasing towards the end of the paroxysmal series. Crystals with normal zoning profiles are dominant within products erupted during the Strombolian activity, but little represented during paroxysmal eruptions. Reverse zoning shows a bimodal distribution over time with two frequency peaks coinciding with the eruptions of July 4 and August 4, and no substantial differences between the Strombolian and the paroxysmal phase. Finally, the presence of complex zoning is quite scattered over the period.

## 5 Discussion

### 5.1 Magma transfer and timescales

A conspicuous literature exists on the composition and zoning of olivine crystals from volcanic products erupted at Etna since 1991 CE [Kahl et al. 2011; 2013; 2015; Viccaro et al. 2016; Giuffrida and Viccaro 2017; Kahl et al. 2017; Cannata et al. 2018; Viccaro et al. 2019; Borzi et al. 2020; Giuffrida et al. 2021; 2023]. Since the pioneering work of Kahl et al. [2011], the study and correlation of olivine zoning coupled with thermodynamic modeling has enabled the refining of the plumbing system internal structure as composed by multiple magmatic environments, which reflect the crystallization conditions of distinct olivine populations. Each environment was defined by stable conditions of pressure, temperature, oxygen fugacity, and magma volatile content ($P$-$T$-$fO_2$-$X$) allowing the growth of homogeneous olivine. Thermodynamic constraints on olivine crystallization have been provided for various eruptive periods at Etna, as for 1991–2008 [Kahl et al. 2015] and 2011–2013 period [Giuffrida and Viccaro 2017]. The most recent constraints come from Giuffrida et al. [2023], who simulate magma differentiation throughout the decade 2011–2022, therefore providing crystallization conditions also for olivine populations of the 2015–2016 and 2020–2022 paroxysmal sequences. These authors defined six magmatic environments associated with compositionally distinct olivine populations, named $M_x$ (Fo>84), $M_{00}$ ($Fo_{84–83}$), $M_0$ ($Fo_{82–80}$), $M_{1a}$ ($Fo_{79–77}$), $M_{1b}$ ($Fo_{76–74}$), and $M_2$ ($Fo_{73–68}$). $P$, $T$, $fO_2$ and volatile contents characterizing each environment are reported in Table 2. In this study, we refer to these most recent constraints to thermodynamically characterize the three olivine core populations found within the 2024 tephra erupted at VOR. In accordance with results from thermodynamic modeling, we assume that crystals belonging to OP1 ($Fo_{80–84}$) formed under $P$-$T$-$fO_2$-$X$ conditions encompassing the magmatic environments $M_{00}$ and $M_0$. The population OP2 ($Fo_{75–79}$) is the most abundant and includes olivine cores that match those associated with the environments $M_{1a}$ and $M_{1b}$. Finally, the most evolved population, OP3 ($Fo_{68–73}$), well overlaps the range of olivine compositions crystallizing at the conditions of $M_2$.

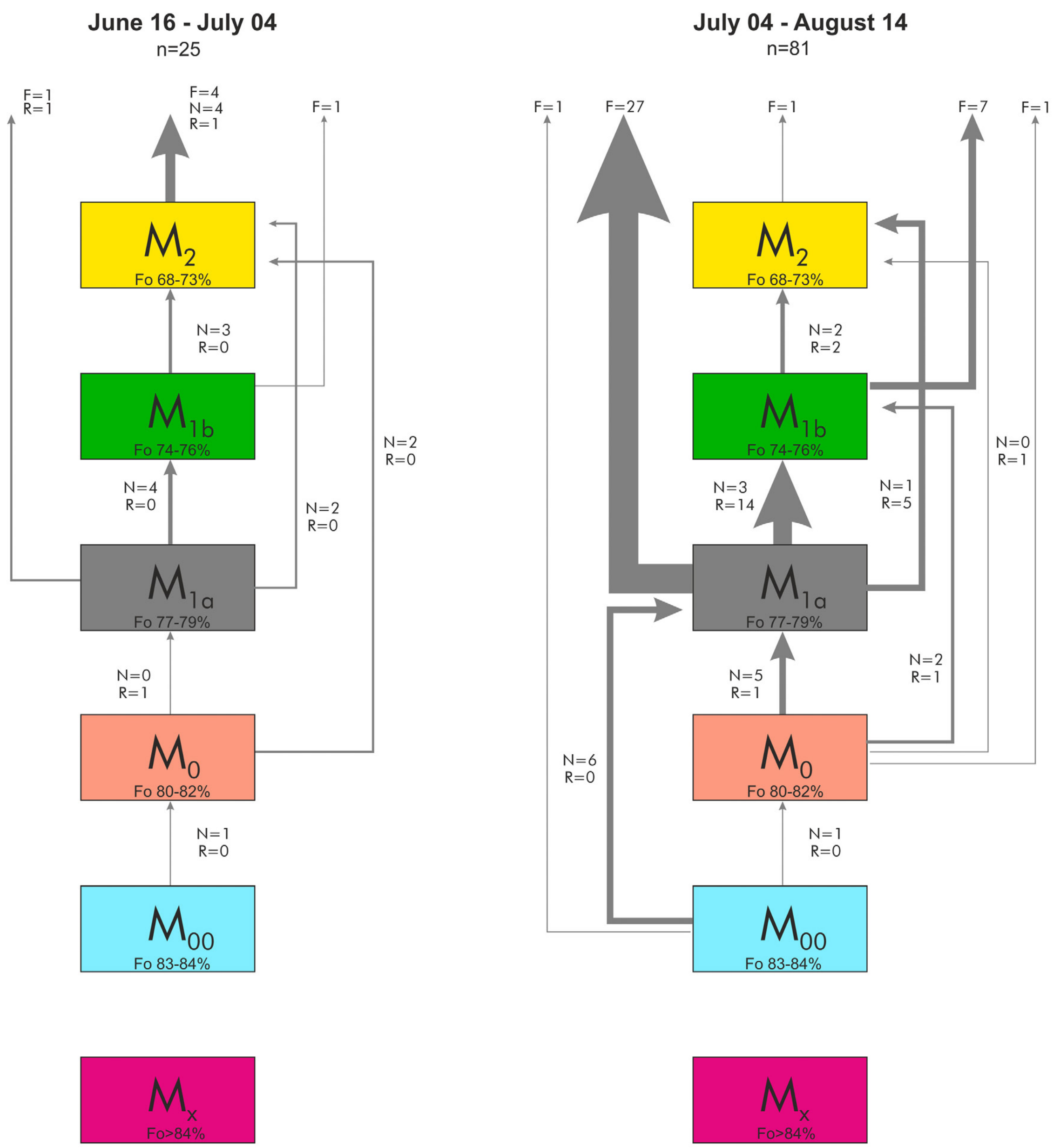


Figure 8: System analysis diagrams for the 2024 periods June 16 to July 4 and July 4 to August 14 illustrating the magma connections between magmatic environments (MEs). Colored boxes represent the MEs (see Table 2 for thermodynamic parameters). The thickness of the grey arrows is proportional to the number of observed transfers and is normalized to the maximum transfer frequency detected across the two periods (i.e. $M_{1a}$—surface during July 4 to August 14). The labels N, R, and F indicate normal, reverse, and flat zoning associated with each transfer.

While growing, olivine can develop chemical zoning in response to changes of the physical-chemical conditions of the host melt during storage and ascent, essentially due to fractionation or magma mixing [Streck 2008]. As such, the spectrum of Fo zoning patterns recognized in our samples can be used to track the polybaric crystallization of an olivine from one environment to another, thus reconstructing the history of migration until its final eruption at the surface. In this study, we have used system analysis diagrams [cf. Kahl et al. 2011; 2015] to illustrate crystal movements and connections between environments in the period June 16 to August 14, as derived from the analysis of olivine core composition and associated zoning (Figure 8). Specifically, system analysis diagrams were constructed for the pre-sequence events (i.e. the Strombolian phase) of June 16 to July 4 and for the paroxysmal sequence of July 4 to August 14.

Most of the crystals erupted during the Strombolian activity of June 16 to July 4 preserve normally zoned rims at $Fo_{68–73}$ (Figure 8), but core compositions indicating early crystallization in various environments, from $M_0$ to $M_{1b}$. This suggests multiple magmatic inputs from the deep portions of the feeding system, extending to depths of ~6.5 km b.s.l., into the

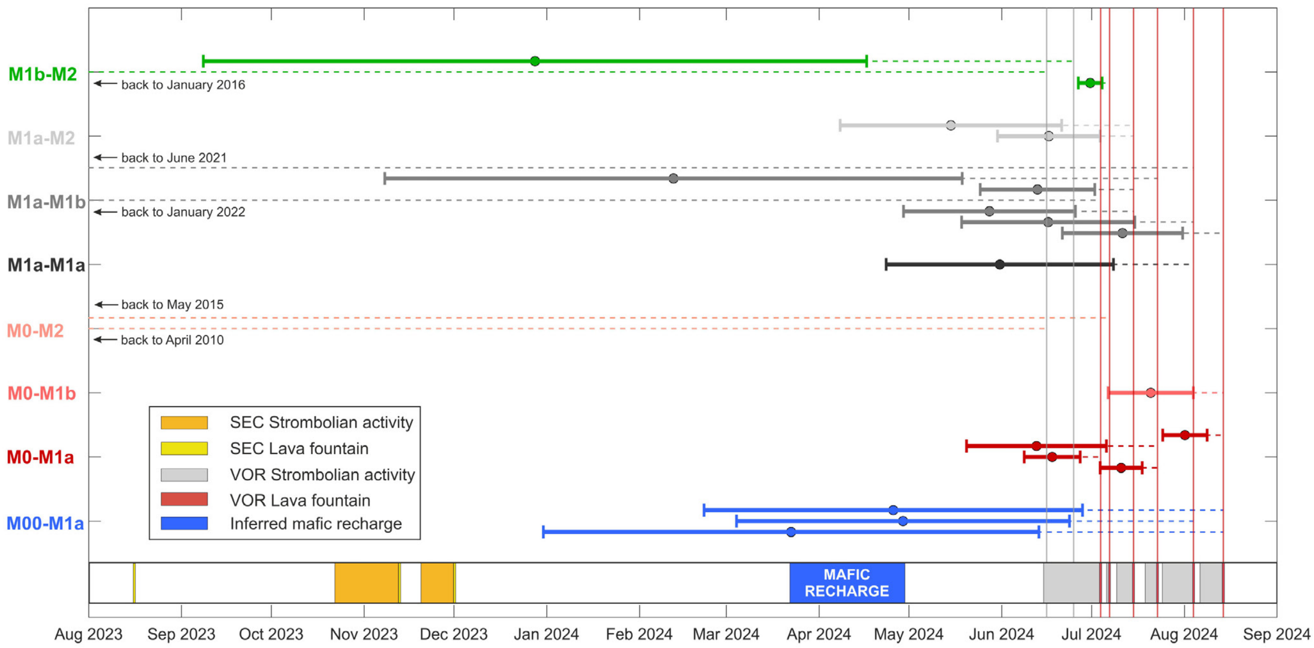


Figure 9: Timeline of the volcanic activity at VOR from June 16 to August 14, 2024 highlighting the key episodes of magmatic intrusion. Vertical grey and red lines represent the sampling date for products of the Strombolian phase and of the paroxysmal events, respectively. The $y$-axis reports the magma transfers inferred from olivine zoning, arranged in order of decreasing depth. Colored dots and horizontal error bars (1σ, see Section 3.2 for details) represent the timescales of the corresponding magma transfers obtained from Fe–Mg diffusion modeling in olivine, with the dotted horizontal lines extending forward in time toward the eruptive event that released each crystal. Some timescales extend beyond the plotted interval; in these cases, the transfer time is marked by a black arrow at the margin of the figure.

crustal interval corresponding to the $M_2$ and $M_{1b}$ magmatic environments (i.e. ~2 km a.s.l.–2 km b.s.l.; cf. Giuffrida et al. [2023]). This interpretation is reinforced by the analysis of glasses for the same period of activity. Indeed, we have observed that glass compositions become progressively more mafic from June 16 to the onset of paroxysmal eruptions on July 4. This supports the idea that the Strombolian phase was fed by subsequent inputs of fresh mafic magmas that progressively mixed with the resident one, and gradually replaced it. The observed glass compositional variability of such kind has been also explained by ascent-related kinetic processes through experimental results [Musu et al. 2026]. However, although these factors may have contributed, the petrological, geochemical, and geophysical datasets available for the recent eruptive sequences at Etna have consistently highlighted the occurrence of recurrent mafic recharge events, leading to the progressive replenishment of the upper plumbing system [e.g. Cannata et al. 2018; Giuffrida et al. 2023; Cardone et al. 2024; Corsaro et al. 2024; Bonaccorso et al. 2025; Salerno et al. 2025]. The crystal chemistry record presented in this study is fully consistent with this long-recognized behavior at Etna, and unequivocally points to the involvement of mafic magma inputs also during the 2024 sequence. Taken together, these observations support mafic recharge as the interpretation that best reconciles our observations on olivine zoning with the glass compositional variations.

The system diagram analysis for the explosive phase of July 4 to August 14 indicates a substantially different scenario. Only a minor proportion of crystals belonging to OP1 and OP2 record normal zoning with decreasing Fo content to $Fo_{68-73}$ (Figure 8), which coincides with the composition of $M_2$. Rather, the OP1 ($Fo_{80-84}$) population is mainly normally zoned with rims in the range $Fo_{74-79}$ (i.e. $M_{1a}$–$M_{1b}$), while OP2 ($Fo_{75-79}$) is dominated by non-zoned crystals and, subordinately, by reversed zoned rims towards more evolved compositions. The majority of crystals of the paroxysmal phase record these zoning patterns. This suggests that the section of the plumbing system between $M_{1a}$ and $M_{1b}$, extending to depths of 0.5 km a.s.l.–5.8 km b.s.l. (i.e. 70–235 MPa; Giuffrida et al. [2023]), was particularly active, accommodating most of mafic magmas coming from the deepest environments $M_0$ and $M_{00}$. The mafic replenishment into the $M_{1a}$–$M_{1b}$ region may have triggered the ascent of the resident magma towards the shallowest environment or directly towards the surface, as also indicated by the abundance of non-zoned $Fo_{75-79}$ crystals in these products.

Results from olivine zoning provide a picture that correlates well with information coming from geophysics. Overall, the high abundance of chemically homogeneous olivine cores at $Fo_{76-77}$ (Figure 5) support the evidence of a main storage region located between $M_{1a}$ and $M_{1b}$ and centered at ~2.7 km b.s.l. The $M_{1a}$–$M_{1b}$ crustal interval partially overlaps the location of an intermediate storage zone inferred by the deformation sources modeled for the mid- to long-term recharging-discharging phases investigated in previous studies [Aloisi et al. 2018; Palano et al. 2024] and by seismic to-

Table 3: Diffusion modeling results for olivine crystals from ash and lapilli erupted during the 2024 paroxysmal sequence at the Voragine crater (VOR) of Mt. Etna volcano. Timescales ($\Delta t$, days) and relative uncertainties ($\pm\sigma$) were calculated for each zoned portion of the crystals (N: normal; R: reverse) and Fo content at core and rim of the modeled crystals is shown. Temperature ($T$), pressure ($P$) and oxygen fugacity ($fO_2$) used in each diffusion model are reported (the rationale is described in Section 3.2). The inferred magma transfers indicate the magmatic environments of the magmas that mixed to produce the modeled compositional gradients.

| Crystal | Zoning | Fo% Core | Fo% Rim | $T$ (°C) | $P$ (MPa) | $\log_{10} fO_2$ (bar) | Transfer | $\Delta t$ (days) | $\pm\sigma$ |
|---|---|---|---|---|---|---|---|---|---|
| VOR_160624_Ol1 | N | 81.5 | 71.0 | 1065 | 50 | -10.90 | $M_0$–$M_2$ | 5186 | 3250 |
| VOR_160624_Ol3 | N | 74.4 | 70.4 | 1065 | 50 | -10.90 | $M_{1b}$–$M_2$ | 3071 | 1459 |
| VOR_250624_Ol2 | N | 71.5 | 70.5 | 1077 | 50 | -10.66 | $M_{1b}$–$M_2$ | 180 | 111 |
| VOR_040724_STR_Ol12 | R | 79.1 | 76.6 | 1121 | 115 | -9.16 | $M_{1a}$–$M_0$ | 16 | 9 |
| VOR_040724B_Ol2 | R | 75.0 | 77.5 | 1088 | 115 | -10.51 | $M_{1b}$–$M_{1a}$ | 898 | 544 |
| VOR_070724A _Ol1 | R | 69.5 | 80.9 | 1065 | 50 | -10.90 | $M_2$–$M_0$ | 3337 | 2091 |
| VOR_070724A _Ol8 | N | 76.5 | 72.7 | 1077 | 50 | -10.66 | $M_{1b}$–$M_2$ | 6 | 4 |
| VOR_150724A_Ol9 | N | 76.6 | 76.6 | 1088 | 50 | -10.00 | $M_{1a}$–$M_2$ | 28 | 17 |
| VOR_150724B_Ol1 | N | 77.4 | 74.4 | 1099 | 115 | -9.96 | $M_{1a}$–$M_{1b}$ | 32 | 19 |
| VOR_150724B_Ol7 | R | 72.5 | 77.9 | 1088 | 50 | -10.00 | $M_2$–$M_{1a}$ | 61 | 37 |
| VOR_150724B_Ol8 | R | 73.1 | 75.7 | 1099 | 50 | -9.96 | $M_{1b}$–$M_{1a}$ | 48 | 29 |
| VOR_230724_Ol1 | N | 80.1 | 75.5 | 1121 | 207 | -9.16 | $M_0$–$M_{1a}$ | 40 | 23 |
| VOR_230724_Ol2 | R | 75.1 | 77.4 | 1099 | 115 | -9.96 | $M_{1b}$–$M_{1a}$ | 162 | 96 |
| VOR_230724_Ol16 | N | 82.0 | 76.9 | 1121 | 207 | -9.16 | $M_0$–$M_{1a}$ | 12 | 7 |
| VOR_040824A_Ol1 | R | 76.3 | 78.2 | 1099 | 115 | -9.96 | $M_{1b}$–$M_{1a}$ | 49 | 29 |
| VOR_040824A_Ol7 | N | 83.2 | 77.3 | 1127 | 207 | -8.07 | $M_{00}$–$M_{1a}$ | 97 | 56 |
| VOR_040824B_Ol2 | R | 75.7 | 78.1 | 1088 | 115 | -10.51 | $M_{1b}$–$M_{1a}$ | 1132 | 686 |
| VOR_040824B_Ol3 | R | 76.7 | 74.8 | 1110 | 207 | -9.73 | $M_{1a}$–$M_{1a}$ | 65 | 38 |
| VOR_140824A_Ol7 | R | 75.5 | 78.6 | 1110 | 115 | -9.21 | $M_{1b}$–$M_0$ | 24 | 14 |
| VOR_140824A_Ol14 | N | 83.1 | 77.0 | 1127 | 207 | -8.07 | $M_{00}$–$M_{1a}$ | 110 | 63 |
| VOR_140824A_Ol15 | N | 82.3 | 75.7 | 1121 | 207 | -9.16 | $M_0$–$M_{1a}$ | 13 | 7 |
| VOR_140824A_Ol17 | R | 75.8 | 77.7 | 1099 | 115 | -9.96 | $M_{1b}$–$M_{1a}$ | 34 | 20 |
| VOR_140824B_Ol3 | N | 83.6 | 78.7 | 1127 | 207 | -8.07 | $M_{00}$–$M_{1a}$ | 144 | 83 |

mography [De Gori et al. 2021; Del Piccolo et al. 2025]. In particular, the upper section of this region coinciding with the $M_{1b}$ environment (approximately between 1 km a.s.l. and 2 km b.s.l.) is consistent with the deflation sources identified for the most energetic lava fountain events of 2015–2016 and 2024 by Bonaccorso et al. [2025]. By applying a numerical finite-element method to strain data, these authors located the deflation source at depths of ~0.5–1.0 km b.s.l., corresponding to the $M_{1b}$ magmatic environment. In this framework, it is worth noting that deformation models applied over longer time intervals (and encompassing multiple paroxysmal events) using GNSS data during the 2015–2016 VOR activity placed the deflation sources at greater depth of ~4.5–5.0 km b.s.l. [e.g. Aloisi et al. 2017; Cannata et al. 2018], which is consistent with the location of $M_{1a}$ environment identified by petrology.

The application of diffusion modeling on zoned olivine has provided time constraints on magma dynamics that fed the 2024 paroxysmal sequence at VOR (Table 3; Supplementary Material 3). Our dataset includes a few crystals providing long diffusion timescales on the order of 8.4–9.1 and 2.5–3.1 years and diffusive relaxation at the conditions of $M_{1b}$ and $M_2$. This suggests prolonged periods of storage in the shallow plumbing system, during which these crystals continued to chemically re-equilibrate with the surrounding melt. These long timescales essentially refer to crystals erupted at the early stage of activity, between June 16 and July 7. In addition, volcanic tephra erupted during this early phase has shown the presence of abundant glomerocrysts of evolved ($Fo_{73-70}$) olivines. We have interpreted these features as the possible consequence of the progressive dismantling of a crystal mush that likely obstructed the volcanic conduit before the beginning of volcanic activity in June 2024.

With the exception of these few cases, all the other crystals provide timescales in the range 6–180 days (Figure 9; Table 3). Specifically, the most mafic olivines ($Fo_{84}$) associated with the environment $M_{00}$ provide timescales of 3–5 months following diffusive relaxation at the conditions of $M_{1a}$. This indicates an early event of mafic magma ascent from deep levels of the feeding system (i.e. $M_{00}$) which occurred in the period between the end of March and end of April 2024.

The arrival of new magma into the intermediate plumbing system seems to have reactivated the resident $M_{1a}$ magma and triggered its ascent, which eventually resulted in the progressive remobilization of more evolved melts stored in the upper reservoirs. The process is testified by many olivines from the paroxysmal sequence that record chemical relaxation at various magmatic conditions, including $M_{1a}$, $M_{1b}$, and $M_2$, and provide timescales of 1–2 months, consistent with magma migration between the end of May and the first half of June 2024, therefore preceding the onset of the paroxysmal sequence at VOR. Finally, very short timescales of 1–2 weeks point to some episodes of syn-eruptive magma ascent during the ongoing activity in July 2024 (Figure 9; Table 3).

### 5.2 The 2024 sequence at Voragine compared to past activity

The eruptive dynamics inferred from the petrology of the 2024 volcanic products erupted at VOR differ substantially from those observed for the 2015–2016 explosive sequences at the same summit crater, which were investigated by Cannata et al. [2018] using the same petrological approach adopted in this study. The comparison of the two datasets highlights significant differences in the relative abundances of olivine populations, location of the storage zones that accommodate magma prior to eruption and in the timing of magma transfers feeding eruptions. For instance, OP1 ($Fo_{80-84}$) compositions are poorly represented within products of the 2024 sequence, whereas they were particularly abundant in products of the 2015–2016 activity. In contrast, OP2 ($Fo_{74-79}$) accounts for more than twice the proportion of crystals in 2024 compared to 2015–2016. One of the most remarkable features of the 2015–2016 activity was the eruption of volcanic tephra bearing some of the most mafic olivine (Fo>85) erupted at Etna in recent times [cf. Cannata et al. 2018; Giuffrida et al. 2023], evidence of the activation of a primitive magmatic environment, named Mx, encompassing high magmatic pressures (>650 MPa) and temperatures [Giuffrida and Viccaro 2017]. Aside from VOR, the observation of such mafic olivine compositions was limited to just a few eruptions of the recent record of Etna, such as the paroxysm of August 2014 and February 2021 at SEC [Viccaro et al. 2016; Giuffrida et al. 2023], but completely lacks in the products of the 2024 sequence. The petrology of recently erupted products has highlighted how the Etna plumbing system during powerful explosive phases is capable of draining efficiently and over very short times most of the primitive magmas injected into the deepest storage region (>13 km b.s.l.) and transfer it directly to the surface. In this context, timescales of magma movements associated with the onset of the 2015–2016 paroxysmal eruptions are much faster than those registered during 2024 for all the connections between magmatic environments (days to weeks vs. weeks to months, respectively). Similar fast dynamics were also observed for the powerful paroxysmal sequence of 2020–2022 at SEC [Giuffrida et al. 2023]. The distribution of olivine compositions and zoning profiles for the 2024 activity suggests, instead, propensity for magmas to accumulate and temporarily reside in intermediate to shallow storage zones (~0.5 km a.s.l.–5.8 km b.s.l.) before eruption, which contrasts with the fast dynamics typically preceding the development of other recent paroxysmal eruptions at Etna.

The reawakening of VOR has concluded a three-year-long period dominated by the activity of SEC. In this framework, the observed magma dynamics may reflect a structural reorganization of the volcanic system, whereby the lack of major magma accumulation in the uppermost reservoir may have favored the ascent of magma through the central conduit system that fed directly VOR, while hindering the drainage of magma toward the SEC.

## 6 Conclusions

The petrological evidence of eruptive products from the VOR crater of Mt. Etna, collected before and during the June to August 2024 activity, provides insights into the dynamics of the magmatic feeding system and the magma transfers that led to the development of the paroxysmal sequence. Our results indicate the arrival of a mafic magma coming from depths of ~6–8 km b.s.l. ($M_{00}$–$M_0$) in the period between late March and late April 2024. This event triggered the reactivation, in sequence, of multiple magma volumes distributed at various depths across the intermediate-shallow portion of the plumbing system.

In the recent past, the reawakening of the VOR crater has caused significant changes in the structural configuration of the volcano, which has in turn influenced the eruptive behavior of the subsequent years. The powerful paroxysmal eruptions of 2015–2016 marked the transition to a period of long-term inflationary recharge regime that anticipated the beginning of a period of activity dominated by effusive eruptions for many years [cf. Viccaro et al. 2019; Borzi et al. 2020; Giuffrida et al. 2021]. More recently, the modest but persistent activity at VOR between 2019–2020 also preceded the resumption of paroxysmal activity at the summit area, culminating in the extraordinary sequence of 62 lava fountain episodes that occurred at the SEC between late 2020 and early 2022 [Giuffrida et al. 2023], after a four-year period characterized by the absence of energetic eruptions at the volcano.

The intense eruptive episodes at VOR during the summer of 2024 have already provided other evidence of significant shifts in the patterns of the ensuing activity, which became comparatively modest during 2025. At the time of writing, the last remarkable event linked to the VOR activity is related to the reactivation of the NEC at the end of 2025, where the two lava fountaining episodes that occurred on December 27 ended a 28-year hiatus of paroxysmal activity at this crater. Indeed, these events were also accompanied by the opening of an explosive vent and an eruptive fissure on the eastern flank of the VOR, suggesting its structural control in the magma drainage throughout the conduit system. Because of these possible implications, any renewed activity at VOR requires to be closely investigated by the scientific community, and the modes of magma recharge and transfer controlling especially its powerful events should be deciphered in the framework of the volcano dynamics of Etna.

## Author Contributions

Massimiliano Cardone: Conceptualization, Data curation, Methodology, Investigation, Software, Writing—original draft. Giorgio Costa: Investigation, Visualization, Writing—original draft. Marisa Giuffrida: Conceptualization, Investigation, Data curation, Writing—original draft. Marco Viccaro: Conceptualization, Investigation, Project administration, Resources, Supervision, Writing—original draft.

## Acknowledgements

This work was partially supported by the program PIA.CE.RI. 2024–26 funded by the University of Catania, project ReVulTe—Relationships between volcanism and tectonics within the framework of the recent activity of Etna (recipient M.V.). G.C. benefited from a PhD fellowship within the framework of the DM 118/2023—PNRR Mission 4 Investment 4.1 for the project "Mechanisms of formation and emplacement of Pyroclastic Density Currents in mafic volcanic systems". We are really thankful to the handling editor Adam Jeffery and to Federico Casetta and an anonymous reviewer for the constructive comments provided.

## Data Availability

All the data used in this article are included as online supplementary materials.

## Competing Interest

The authors declare that they have no known competing financial interest or personal relationships that could have appeared to influence the work reported in this paper.

## Copyright Notice



## References

Aloisi, M., A. Bonaccorso, F. Cannavò, and G. M. Currenti (2018). "Coupled Short- and Medium-Term Geophysical Signals at Etna Volcano: Using Deformation and Strain to Infer Magmatic Processes From 2009 to 2017". *Frontiers in Earth Science* 6. DOI: 10.3389/feart.2018.00109.

Aloisi, M., M. D'Agostino, K. G. Dean, A. Mostaccio, and G. Neri (2002). "Satellite analysis and PUFF simulation of the eruptive cloud generated by the Mount Etna paroxysm of 22 July 1998". *Journal of Geophysical Research: Solid Earth* 107(B12). DOI: 10.1029/2001jb000630.

Aloisi, M., S. Jin, F. Pulvirenti, and A. Scaltrito (2017). "The December 2015 Mount Etna eruption: An analysis of inflation/deflation phases and faulting processes". *Journal of Geodynamics* 107, pages 34–45. DOI: 10.1016/j.jog.2017.03.003.

Andronico, D. and R. A. Corsaro (2011). "Lava fountains during the episodic eruption of South–East Crater (Mt. Etna), 2000: insights into magma-gas dynamics within the shallow volcano plumbing system". *Bulletin of Volcanology* 73(9), pages 1165–1178. DOI: 10.1007/s00445-011-0467-y.

Andronico, D., A. Cannata, G. Di Grazia, and F. Ferrari (2021). "The 1986–2021 paroxysmal episodes at the summit craters of Mt. Etna: Insights into volcano dynamics and hazard". *Earth-Science Reviews* 220, page 103686. DOI: 10.1016/j.earscirev.2021.103686.

Armienti, P., F. Innocenti, R. Petrini, M. Pompilio, and L. Villari (1989). "Petrology and Sr-Nd isotope geochemistry of recent lavas from Mt. Etna: bearing on the volcano feeding system". *Journal of Volcanology and Geothermal Research* 39(4), pages 315–327. DOI: 10.1016/0377-0273(89)90095-4.

Behncke, B., S. Branca, R. A. Corsaro, E. De Beni, L. Miraglia, and C. Proietti (2014). "The 2011–2012 summit activity of Mount Etna: Birth, growth and products of the new SE crater". *Journal of Volcanology and Geothermal Research* 270, pages 10–21. DOI: 10.1016/j.jvolgeores.2013.11.012.

Behncke, B. and M. Neri (2003). "Cycles and trends in the recent eruptive behaviour of Mount Etna (Italy)". *Canadian Journal of Earth Sciences* 40(10), pages 1405–1411. DOI: 10.1139/e03-052.

Behncke, B., M. Neri, E. Pecora, and V. Zanon (2006). "The exceptional activity and growth of the Southeast Crater, Mount Etna (Italy), between 1996 and 2001". *Bulletin of Volcanology* 69(2), pages 149–173. DOI: 10.1007/s00445-006-0061-x.

Bonaccorso, A., S. D'Amico, M. Mattia, and D. Patanè (2004). "Intrusive Mechanisms at Mt. Etna Forerunning the July-August 2001 Eruption from Seismic and Ground Deformation Data". *Pure and Applied Geophysics* 161(7), pages 1469–1487. DOI: 10.1007/s00024-004-2515-4.

Bonaccorso, A., L. Carleo, G. Currenti, and A. Sicali (2025). "The intense explosive activity of lava fountain sequences from Voragine crater at Etna volcano: new insights through high-precision borehole strain recordings". *Frontiers in Earth Science* 13. DOI: 10.3389/feart.2025.1606006.

Borzi, A. M., M. Giuffrida, F. Zuccarello, M. Palano, and M. Viccaro (2020). "The Christmas 2018 Eruption at Mount Etna: Enlightening How the Volcano Factory Works Through a Multiparametric Inspection". *Geochemistry, Geophysics, Geosystems* 21(10). DOI: 10.1029/2020gc009226.

Caltabiano, T., M. Burton, S. Giammanco, P. Allard, N. Bruno, F. Murè, and R. Romano (2004). "Volcanic gas emissions from the summit craters and flanks of Mt. Etna, 1987–2000". *Mt. Etna: Volcano Laboratory*. American Geophysical Union, pages 111–128. DOI: 10.1029/143gm08.

Cannata, A., G. Di Grazia, M. Giuffrida, S. Gresta, M. Palano, M. Sciotto, M. Viccaro, and F. Zuccarello (2018). "Space-Time Evolution of Magma Storage and Transfer at Mt. Etna Volcano (Italy): The 2015–2016 Reawakening of Voragine Crater". *Geochemistry, Geophysics, Geosystems* 19(2), pages 471–495. DOI: 10.1002/2017gc007296.

Cardone, M., A. Cannata, M. Giuffrida, A. Iozzia, V. Minio, M. Viccaro, and S. Gambino (2024). "Changing magma recharge/discharge dynamics during the 2020–22 lava fountaining activity at Mt. Etna revealed by tilt deformation and volcanic tremor". *Journal of Volcanology and Geothermal Research* 449, page 108074. DOI: 10.1016/j.jvolgeores.2024.108074.

Corsaro, R., D. Andronico, B. Behncke, S. Branca, T. Caltabiano, F. Ciancitto, A. Cristaldi, E. De Beni, A. La Spina, L. Lodato, L. Miraglia, M. Neri, G. Salerno, S. Scollo, and G. Spata (2017). "Monitoring the December 2015 summit eruptions of Mt. Etna (Italy): Implications on eruptive dynamics". *Journal of Volcanology and Geothermal Research* 341, pages 53–69. DOI: 10.1016/j.jvolgeores.2017.04.018.

Corsaro, R. A. and L. Miraglia (2014). "The transition from summit to flank activity at Mt. Etna, Sicily (Italy): Inferences from the petrology of products erupted in 2007–2009". *Journal of Volcanology and Geothermal Research* 275, pages 51–60. DOI: 10.1016/j.jvolgeores.2014.02.009.

Corsaro, R. A., L. Miraglia, I. Arienzo, and V. Di Renzo (2024). "The 2020–2022 paroxysmal episodes of the South-East Crater (Mt. Etna): insights into high-frequency eruptive activity from petrological monitoring". *Bulletin of Volcanology* 86(10). DOI: 10.1007/s00445-024-01770-4.

Corsaro, R. A., L. Miraglia, and M. Pompilio (2007). "Petrologic evidence of a complex plumbing system feeding the July–August 2001 eruption of Mt. Etna, Sicily, Italy". *Bulletin of Volcanology* 69(4), pages 401–421. DOI: 10.1007/s00445-006-0083-4.

Costa, F., R. Dohmen, and S. Chakraborty (2008). "Time Scales of Magmatic Processes from Modeling the Zoning Patterns of Crystals". *Reviews in Mineralogy and Geochemistry* 69(1), pages 545–594. DOI: 10.2138/rmg.2008.69.14.

Costa, F. and S. Chakraborty (2004). "Decadal time gaps between mafic intrusion and silicic eruption obtained from chemical zoning patterns in olivine". *Earth and Planetary Science Letters* 227(3-4), pages 517–530. DOI: 10.1016/j.epsl.2004.08.011.

De Gori, P., E. Giampiccolo, O. Cocina, S. Branca, C. Doglioni, and C. Chiarabba (2021). "Re-pressurized magma at Mt. Etna, Italy, may feed eruptions for years". *Communications Earth & Environment* 2(1). DOI: 10.1038/s43247-021-00282-9.

Del Piccolo, G., B. P. VanderBeek, M. Faccenda, R. Lo Bue, O. Cocina, M. Firetto Carlino, E. Giampiccolo, L. Scarfí, F. Rappisi, T. Gerya, and A. Morelli (2025). "Pressurized magma storage in radial dike network beneath Etna volcano evidenced with P-wave anisotropic imaging". *Communications Earth & Environment* 6(1). DOI: 10.1038/s43247-025-02328-8.

Dohmen, R. and S. Chakraborty (2007). "Fe–Mg diffusion in olivine II: point defect chemistry, change of diffusion mechanisms and a model for calculation of diffusion coefficients in natural olivine". *Physics and Chemistry of Minerals* 34(6), pages 409–430. DOI: 10.1007/s00269-007-0158-6.

Edwards, M. J., L. Pioli, D. Andronico, S. Scollo, F. Ferrari, and A. Cristaldi (2018). "Shallow factors controlling the explosivity of basaltic magmas: The 17–25 May 2016 eruption of Etna Volcano (Italy)". *Journal of Volcanology and Geothermal Research* 357, pages 425–436. DOI: 10.1016/j.jvolgeores.2018.05.015.

Giuffrida, M., M. Cardone, F. Zuccarello, and M. Viccaro (2023). "Etna 2011–2022: Discoveries from a decade of activity at the volcano". *Earth-Science Reviews* 245, page 104563. DOI: 10.1016/j.earscirev.2023.104563.

Giuffrida, M., M. Scandura, G. Costa, F. Zuccarello, M. Sciotto, A. Cannata, and M. Viccaro (2021). "Tracking the summit activity of Mt. Etna volcano between July 2019 and January 2020 by integrating petrological and geophysical data". *Journal of Volcanology and Geothermal Research* 418, page 107350. DOI: 10.1016/j.jvolgeores.2021.107350.

Giuffrida, M. and M. Viccaro (2017). "Three years (2011–2013) of eruptive activity at Mt. Etna: Working modes and timescales of the modern volcano plumbing system from micro-analytical studies of crystals". *Earth-Science Reviews* 171, pages 289–322. DOI: 10.1016/j.earscirev.2017.06.003.

Harris, A. J. and M. Neri (2002). "Volumetric observations during paroxysmal eruptions at Mount Etna: pressurized drainage of a shallow chamber or pulsed supply?" *Journal of Volcanology and Geothermal Research* 116(1-2), pages 79–95. DOI: 10.1016/s0377-0273(02)00212-3.

INGV-OE (2024a). *Bollettino Settimanale sul monitoraggio multiparametrico del vulcano Etna, Rep. N. 28/2024. Published 09/07/2024.* URL: https://www.ct.ingv.it/index.php/monitoraggio-e-sorveglianza/prodotti-del-monitoraggio/bollettini-settimanali-multidisciplinari/919-bollettino-Settimanale-sul-monitoraggio-vulcanico-geochimico-e-sismico-del-vulcano-Etna-del-2024-07-09/file.

– (2024b). *Bollettino Settimanale sul monitoraggio multiparametrico del vulcano Etna, Rep. N. 30/2024. Published 23/07/2024.* URL: https://www.ct.ingv.it/index.php/monitoraggio-e-sorveglianza/prodotti-del-monitoraggio/bollettini-settimanali-multidisciplinari/923-bollettino-Settimanale-sul-monitoraggio-vulcanico-geochimico-e-sismico-del-vulcano-Etna-del-2024-07-23/file.

– (2024c). *Bollettino Settimanale sul monitoraggio multiparametrico del vulcano Etna, Rep. N. 31/2024. Published 30/07/2024.* URL: https://www.ct.ingv.it/index.php/monitoraggio-e-sorveglianza/prodotti-del-monitoraggio/bollettini-settimanali-multidisciplinari/925-bollettino-Settimanale-sul-monitoraggio-vulcanico-geochimico-e-sismico-del-vulcano-Etna-del-2024-07-30/file.

– (2024d). *Bollettino Settimanale sul monitoraggio multiparametrico del vulcano Etna, Rep. N. 32/2024. Published 06/08/2024.* URL: https://www.ct.ingv.it/index.php/monitoraggio-e-sorveglianza/prodotti-del-monitoraggio/bollettini-settimanali-multidisciplinari/929-bollettino-Settimanale-sul-monitoraggio-vulcanico-geochimico-e-sismico-del-vulcano-Etna-del-2024-08-06/file.

– (2024e). *Bollettino Settimanale sul monitoraggio multiparametrico del vulcano Etna, Rep. N. 34/2024. Published 20/08/2024.* URL: https://www.ct.ingv.it/index.php/monitoraggio-e-sorveglianza/prodotti-del-monitoraggio/bollettini-settimanali-multidisciplinari/934-bollettino-Settimanale-sul-monitoraggio-vulcanico-geochimico-e-sismico-del-vulcano-Etna-del-2024-08-20/file.

Kahl, M., S. Chakraborty, F. Costa, and M. Pompilio (2011). "Dynamic plumbing system beneath volcanoes revealed by kinetic modeling, and the connection to monitoring data: An example from Mt. Etna". *Earth and Planetary Science*

*Letters* 308(1-2), pages 11–22. DOI: 10.1016/j.epsl.2011.05.008.

Kahl, M., S. Chakraborty, F. Costa, M. Pompilio, M. Liuzzo, and M. Viccaro (2013). "Compositionally zoned crystals and real-time degassing data reveal changes in magma transfer dynamics during the 2006 summit eruptive episodes of Mt. Etna". *Bulletin of Volcanology* 75(2). DOI: 10.1007/s00445-013-0692-7.

Kahl, M., S. Chakraborty, M. Pompilio, and F. Costa (2015). "Constraints on the Nature and Evolution of the Magma Plumbing System of Mt. Etna Volcano (1991–2008) from a Combined Thermodynamic and Kinetic Modelling of the Compositional Record of Minerals". *Journal of Petrology* 56(10), pages 2025–2068. DOI: 10.1093/petrology/egv063.

Kahl, M., M. Viccaro, T. Ubide, D. J. Morgan, and D. B. Dingwell (2017). "A Branched Magma Feeder System during the 1669 Eruption of Mt Etna: Evidence from a Time-integrated Study of Zoned Olivine Phenocryst Populations". *Journal of Petrology* 58(3), pages 443–472. DOI: 10.1093/petrology/egx022.

La Delfa, S., G. Patanè, R. Clocchiatti, J.-L. Joron, and J.-C. Tanguy (2001). "Activity of Mount Etna preceding the February 1999 fissure eruption: inferred mechanism from seismological and geochemical data". *Journal of Volcanology and Geothermal Research* 105(1-2), pages 121–139. DOI: 10.1016/s0377-0273(00)00249-3.

Lo Bue, R., F. Rappisi, M. Firetto Carlino, E. Giampiccolo, O. Cocina, B. P. Vanderbeek, and M. Faccenda (2024). "Crustal Structure of Etna Volcano (Italy) From P-Wave Anisotropic Tomography". *Geophysical Research Letters* 51(13). DOI: 10.1029/2024gl108733.

Métrich, N., P. Allard, N. Spilliaert, D. Andronico, and M. Burton (2004). "2001 flank eruption of the alkali- and volatile-rich primitive basalt responsible for Mount Etna's evolution in the last three decades". *Earth and Planetary Science Letters* 228(1-2), pages 1–17. DOI: 10.1016/j.epsl.2004.09.036.

Musu, A., F. Vetere, T. Griffiths, M. Petrelli, R. A. Corsaro, A. Pisello, S. Peres, D. Perugini, and L. Caricchi (2026). "Experimental Constraints on the Impact of Shear Strain Rate on Early Crystallisation Dynamics and Residual Glass Composition: Implication for Magma Evolution in Natural Systems". *Journal of Petrology* 67(3). Edited by J. Hammer. DOI: 10.1093/petrology/egag015.

Palano, M., G. Pezzo, and C. Chiarabba (2024). "Magma budget, plutonic growth and lateral spreading at Mt. Etna". *Communications Earth & Environment* 5(1). DOI: 10.1038/s43247-024-01267-0.

Paonita, A., M. Liuzzo, G. Salerno, C. Federico, P. Bonfanti, A. Caracausi, G. Giuffrida, A. La Spina, T. Caltabiano, S. Gurrieri, and G. Giudice (2021). "Intense overpressurization at basaltic open-conduit volcanoes as inferred by geochemical signals: The case of the Mt. Etna December 2018 eruption". *Science Advances* 7(36). DOI: 10.1126/sciadv.abg6297.

Patanè, D., P. De Gori, C. Chiarabba, and A. Bonaccorso (2003). "Magma Ascent and the Pressurization of Mount Etna's Volcanic System". *Science* 299(5615), pages 2061–2063. DOI: 10.1126/science.1080653.

Pompilio, M., A. Bertagnini, P. Del Carlo, and A. Di Roberto (2017). "Magma dynamics within a basaltic conduit revealed by textural and compositional features of erupted ash: the December 2015 Mt. Etna paroxysms". *Scientific Reports* 7(1). DOI: 10.1038/s41598-017-05065-x.

Salerno, G., A. La Spina, P. Allard, L. Guerrieri, S. Corradini, G. Di Grazia, L. Merucci, P. Bonfanti, D. Stelitano, R. Maugeri, F. Murè, and P. Principato (2025). "The February–April 2021 sequence of lava fountain paroxysms on Mt Etna: source mechanism deciphered from ground-based and satellite survey of volcanic gas emissions". *Bulletin of Volcanology* 87(11). DOI: 10.1007/s00445-025-01877-2.

Shea, T., F. Costa, D. Krimer, and J. E. Hammer (2015a). "Accuracy of timescales retrieved from diffusion modeling in olivine: A 3D perspective". *American Mineralogist* 100(10), pages 2026–2042. DOI: 10.2138/am-2015-5163.

Shea, T., K. J. Lynn, and M. O. Garcia (2015b). "Cracking the olivine zoning code: Distinguishing between crystal growth and diffusion". *Geology* 43(10), pages 935–938. DOI: 10.1130/g37082.1.

Streck, M. J. (2008). "Mineral Textures and Zoning as Evidence for Open System Processes". *Reviews in Mineralogy and Geochemistry* 69(1), pages 595–622. DOI: 10.2138/rmg.2008.69.15.

Ubide, T. and B. S. Kamber (2018). "Volcanic crystals as time capsules of eruption history". *Nature Communications* 9(1). DOI: 10.1038/s41467-017-02274-w.

Viccaro, M., M. Giuffrida, F. Zuccarello, M. Scandura, M. Palano, and S. Gresta (2019). "Violent paroxysmal activity drives self-feeding magma replenishment at Mt. Etna". *Scientific Reports* 9(1). DOI: 10.1038/s41598-019-43211-9.

Viccaro, M., F. Zuccarello, A. Cannata, M. Palano, and S. Gresta (2016). "How a complex basaltic volcanic system works: Constraints from integrating seismic, geodetic, and petrological data at Mount Etna volcano during the July–August 2014 eruption". *Journal of Geophysical Research: Solid Earth* 121(8), pages 5659–5678. DOI: 10.1002/2016jb013164.